



**HAL**  
open science

## In situ x-ray phase-contrast imaging of spark erosion of aeronautical fasteners

Amélie Jarnac, Rafael Sousa Martins, Clément Zaepffel, Fabien Tholin, Patrice Blanchet, Victor Désangles, Laureen Guitard, Adrien Stolidi, Philippe Lalande

► **To cite this version:**

Amélie Jarnac, Rafael Sousa Martins, Clément Zaepffel, Fabien Tholin, Patrice Blanchet, et al.. In situ x-ray phase-contrast imaging of spark erosion of aeronautical fasteners. ICOLSE 2022 - International Conference On Lightning and Static Electricity, Sep 2022, Madrid, Spain. hal-03878296

**HAL Id: hal-03878296**

**<https://hal.science/hal-03878296v1>**

Submitted on 29 Nov 2022

**HAL** is a multi-disciplinary open access archive for the deposit and dissemination of scientific research documents, whether they are published or not. The documents may come from teaching and research institutions in France or abroad, or from public or private research centers.

L'archive ouverte pluridisciplinaire **HAL**, est destinée au dépôt et à la diffusion de documents scientifiques de niveau recherche, publiés ou non, émanant des établissements d'enseignement et de recherche français ou étrangers, des laboratoires publics ou privés.

# In situ x-ray phase-contrast imaging of spark erosion of aeronautical fasteners

A. Jarnac<sup>1</sup>, R. Sousa Martins<sup>1</sup>, C. Zaepffel<sup>1</sup>, F.Tholin<sup>1</sup>, P. Blanchet<sup>1</sup>, V. Désangles<sup>1</sup>, L. Guitard<sup>2,3</sup>, A. Stolidi<sup>2</sup>, P. Lalande<sup>1</sup>

<sup>1</sup> Université Paris-Saclay, ONERA, DPHY, F-91123 Palaiseau, France

<sup>2</sup> Université Paris-Saclay, CEA, List, F-91120 Palaiseau, France

<sup>3</sup> Université Paris-Saclay, ONERA, DOTA, F-91123 Palaiseau, France  
{amelie.jarnac, philippe.lalande}@onera.fr

**Keywords:** fastener, spark erosion, X-ray phase contrast imaging, X-ray phase tomography.

## 1. ABSTRACT

In the context of lightning strike impacting aeronautical fasteners, we investigate the in situ behaviour of fasteners subject to a current level of a few kA by using high-speed X-ray phase-contrast imaging in a synchrotron facility. It reveals that the fastener erosion occurs in two time scales. On a microsecond timescale, hot particles are ejected from cavity walls of the Carbon fibre reinforced polymer due to sparking/arcing phenomena, whereas on a sub-millisecond time scale, the fastener wall is vaporized due to the electrical energy deposited in the arc-fastener interface. The experimental observations have been used as input for an electro-thermal model of electric contact. The estimated vaporised depth is in good agreement with the measured one. The nature of the internal damages has been confirmed by using X-ray phase tomography.

The DOI for the data is the following: 10.15151/ESRF-ES-650701038.

## 2. INTRODUCTION

When lightning strikes an aircraft, the high current injected in the fuselage flows across a large number of titanium fasteners holding panelling in place. At these interfaces, sparking/arcing phenomena can produce pressures of MPa and outgassing with hot particle ejections damaging panelling and fastener [1], which is an important concern for fuel tank safety. Over the last 2 decades the use of Carbon Fiber Reinforced Polymer (CFRP) composites for aircraft panelling has rapidly increased due to its high strength to weight ratio. However, compared to traditionally used aluminium panelling, carbon composites have lower thermal and electrical conductivities, increasing the risk of thermomechanical damage if lightning strikes occur. Hence understanding and then controlling the sparking phenomenon is fundamental for flight safety.

Experimental studies of sparking phenomenon are very complex to address because (i) it needs a pulse power driver of a few kA for a few  $\mu$ s and (ii) it is encapsulated inside a microscopic cavity. So far, only indirect or invasive measurements have been performed. Sousa Martins et al. [2] characterized the carbon-metallic contact resistance over time in order to derive the dissipated electrical energy in the fastener. These measurements were correlated to the occurrence of outgassing using external visualisation. Liebscher et al. [1] measured the pressure build up inside the cavity by integrating a pressure sensor in the nut.

In this work, we make the first non-invasive measurement of the behaviour of fasteners subject to lightning currents, using high-speed X-ray phase contrast imaging (XPCI). The fastener geometry is simplified to focus on the basic physics of spark erosion and to optimize the X-ray visualisation. The fastener is subjected to a fraction (3 kA) of the standard D-component lightning current waveform. The dynamic of spark erosion during current injection is recorded by high-speed XPCI. Then, after the lightning, a non-invasive inspection of internal damages is performed using X-ray phase tomography.

## 3. ACRONYMS AND SYMBOLS

CFRP: Carbon Fibre Reinforced Polymer

ESRF: European Synchrotron Radiation Facility

FOV: Field of View

HV: High Voltage

XPCI: X-ray Phase Contrast Imaging

## 4. X-RAY PHASE CONTRASTE IMAGING

In most X-ray imaging techniques, the contrast comes from the wave front attenuation of the X-ray beam when it goes through a material. However, low-Z materials, such as Carbon or gases, are weakly absorbing and exhibit poor contrast. To better distinguish these materials, one can make use of wave front distortions of the X-ray beam induced by the change of refractive index. These techniques are called X-ray phase contrast imaging (XPCI) [3]. If the X-ray beam is spatially coherent, the distortions give rise to interference fringes by near field diffraction just by propagation to the detector (see Fig. 1). It leads to edges and interfaces enhancement and improves the perception of elements with similar absorption. In the case of in-line XPCI (no optical elements are added to the beam path), the fringes amplitude is proportional to the Laplacian of the refractive index profile. It means that steeper is the index gradient, larger is the fringe amplitude.

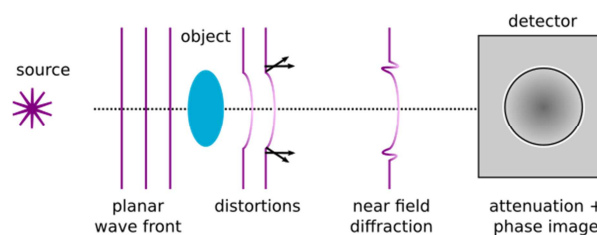


Fig. 1. Principle of in-line phase contrast imaging. A coherent planar wave front is distorted by the object to image. The deviated rays interfere in the near field and give rise to a fringe enhancing the edge of the object.

This imaging technique is particularly interesting for imaging fasteners. Indeed, the cavity is buried, so imaging

needs hard X-ray ( $> 20$  keV), however, the materials (CFRP) or the phenomena (sparking, outgassing) are weakly absorbing at these X-ray energies and happen at interfaces, so imaging needs to be enhanced with phase contrast.

## 5. EXPERIMENTAL SETUPS

### 5.1 Academic fastener assembly

The fastener is composed of a CFRP panel and only two fasteners, allowing for simplified circulation paths of current in the structure (Fig. 2).

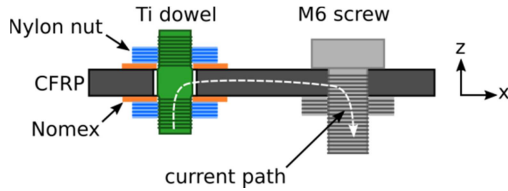


Fig. 2. Scheme of the academic fastener assembly.

The CFRP panel is 4.1 mm-thick and has for dimension  $20 \text{ mm} \times 50 \text{ mm}$ . The panel is made of sixteen plies of align T700 carbon fibres (Toray) with a diameter of  $12 \pm 3 \mu\text{m}$ , surrounded by Epoxy resin M21 (Hexcel) [2]. The successive plies are oriented at  $-45^\circ$  and  $+45^\circ$ . This atypical multilayered panel guaranties that all the plies contribute equally to the transport of current between the two fasteners. The studied cavity is formed by a Titanium dowel with a diameter of 5 mm and a central flat length of 4 mm inserted in a hole with a diameter of 6.5 mm. This configuration has been chosen to facilitate the imaging of the cavity from above (z-direction in Fig. 2). Particular care is taken to centre the fastener on the cavity. The dowel is tightened to the panel by Nylon nuts (to increase X-ray transmission). A dielectric washer made of NOMEX T410 with  $125 \mu\text{m}$  thickness, adjusted to the dowel diameter, is inserted between the nut and the panel to ensure that the current flows inside the dowel and to seal the cavity. The second fastener is a stainless steel M6 screw mounted in interference fit to avoid arcing on this side.

It should be noted that the fastener installation proposed in this work is simplified compare to a real aeronautical assembly. However, these simplifications keep the spark erosion phenomenon representative in order to focus on its basic physics.

### 5.2 Current generator and waveforms

The current generator used in this work has been specially designed by ONERA for use in studies of sparking phenomena in aeronautical fastener cavities induced by lightning strikes. It is a RLC circuit able to deliver a fraction of the standard D-component current waveform as defined in the SAE ARP documents. The generator delivers a single pulse of current with a bi-exponential waveform with a maximum of 3.4 kA. The waveform reaches its maximum in roughly  $14 \mu\text{s}$  and decreases to half of its maximum in  $40 \mu\text{s}$  (see Fig. 3).

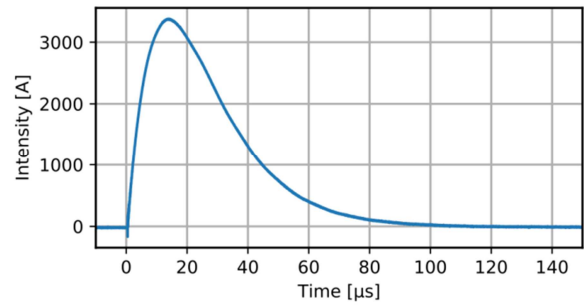


Fig. 3. Pulsed current waveform used in this work, derived from the D-component.

### 5.3 Measurement setups

We performed the experiment at the ID19 beamline of the European Synchrotron Radiation Facility (ESRF) in Grenoble (France) since ultra-high speed, hard X-ray phase contrast imaging, with the possibility to couple a pulsed power driver can only be found here [4]. The experiment was conducted in two stages. First, we recorded the dynamic inside the cavity of a pristine fastener assembly subject to multi kA current at the microsecond time scale by using high-speed XPCI. Then, the damaged fastener is analysed by using phase contrast tomography.

#### 5.3.1 High-speed XPCI

The setup is illustrated in Fig. 4. X-rays are delivered by the ESRF and the point source is located 145 m upstream from the sample. This high distance allows putting the beam in shape in order to get an intense collimated beam with a planar wave front on large field of view (FOV). The generator injects a single 3.4 kA current pulse into the carbon fibre panel through the Titanium dowel (HV+, see Fig. 4b). This cavity is imaged 14 m downstream on a visible high-speed camera (Hyper Vision HPV-X2 from Shimadzu) using a scintillator to convert the X-ray light into visible light. The camera has a sensor made of  $400 \times 250$  pixels, with a pixel size of  $32 \mu\text{m}$ , resulting in a FOV of about  $12 \text{ mm} \times 8 \text{ mm}$  (magnification of 1). The cavity region is recorded at a speed of 500 kHz with an exposure time of 200 ns. To achieve these recording conditions, the white beam (full X-ray spectrum peaked at 30 keV) is use to maximize the photon flux. The injected current is measured using a Rogowski coil current probe from PEM. The camera is synchronised with the generator and starts to acquire  $1 \mu\text{s}$  earlier than the current injection.

#### 5.3.2 Phase contrast tomography

The setup is illustrated in Fig. 5. The tomography is performed with a mounted fastener, previously damaged during the high-speed XPCI acquisition. The sample is located 155 m downstream from the point source and placed vertically into the X-ray path. The beam is polychromatic and the X-ray energy is set to 75 keV with a full width at half maximum of about 20 keV. The damaged cavity is imaged on a PCO edge 5.5 camera using a scintillator. The magnification is 1 and the FOV is  $16.6 \text{ mm} \times 10.7 \text{ mm}$  with a pixel resolution of  $6.5 \mu\text{m}$  (Fig. 5b). The sample is rotated over  $360^\circ$  along the y-axis, with the cavity being at the centre of rotation. The tomogram consists of 5000 images (projections) with an angular increment of  $0.07^\circ$ , each images having for exposure time 50 ms. A phase retrieval algorithm [5] [6] is applied to the projections in order to

enhances the area lacking of contrast by exploiting the phase, and then the tomograms are reconstructed. Due to several assumptions in the retrieval process, it should be noted that the tomogram is not quantitative, but the contrast is related to the change in material density.

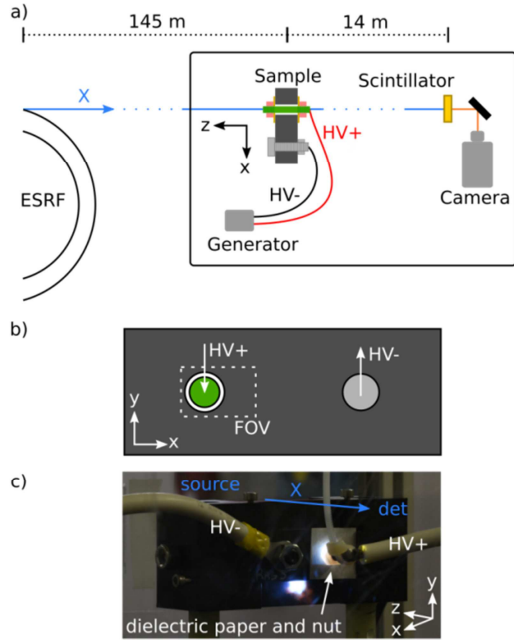


Fig. 4. a) General overview of the setup. X-rays are delivered by the ESRF. The sample is located 145 m downstream from the point source. The cavity under study is aligned into the beam and imaged 14 m further away on a visible high-speed camera (Shimadzu HPV-X2) using a scintillator. b) Scheme of the fastener assembly. The current (HV+) is injected through the studied cavity and returns (HV-) through the M6 screw to the generator. The FOV (dashed white line) is 12 mm x 8 mm. c) Photograph of the fastener assembly during current injection.

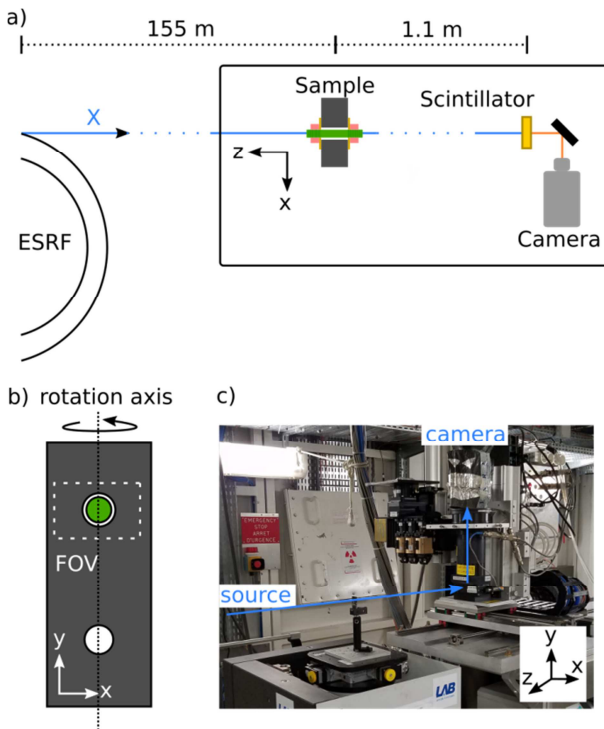


Fig. 5. a) General overview of the setup. The fastener is located 155 m downstream from the X-ray point source. The damaged cavity is imaged

1.1 m further away on a sCMOS camera (PCO edge 5.5) using a scintillator.

b) Scheme of the fastener assembly. The FOV (dashed white line) is 16.6 mm x 10.7 mm. The axis of rotation is along y. c) Photography of the setup.

## 6. RESULTS AND DISCUSSION

The image of the cavity as recorded by the high-speed XPCI setup can be seen in Fig. 6. We can see the dowel in black, highly attenuating the beam, since it is a Titanium rod. The HV+ cable, on the left, is fastened to the dowel by a Nylon cable tie. Thanks to phase contrast, edges are emphasized: the cable tie (visible teeth around the dowel), the Nylon nuts and the cavity seen through the nuts (marked by the two white arrows). In the image, the current flows from left to right-hand side.

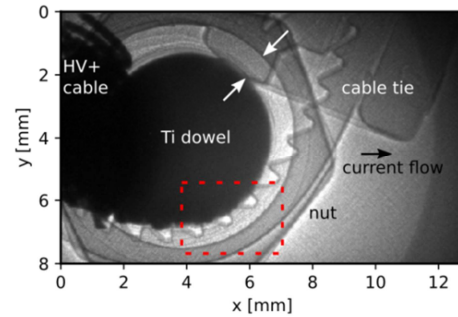


Fig. 6. Top view of the cavity recorded by the high-speed XPCI setup. One can see the dowel, the edge of the nuts, the HV cable coming from the left of the image and the Nylon cable tie used to attach it. The cavity is marked by the two white arrows. The current flows from left to right. The red dashed box is the zoomed area reported in Fig. 7.

The dynamic of the cavity during current injection, is reported in Fig. 7. It shows for selected delays a zoomed area from Fig. 6 (see red dashed box) since most of the dynamic happens here. Indeed, this is the shortest Ti-CFRP distance, since the dowel is not perfectly centered on the cavity. This behaviour is confirmed by the edge glow only visible at the bottom of the CFRP panel in Fig. 4c. To enhance the spark erosion evolution, we plot the difference  $\Delta I(\tau) = I(\tau) - I(\tau = -1 \mu s)$ , where  $I(\tau)$  is the contrast intensity of the image at the delay  $\tau$ . This information refers to the colour bar. To better locate phenomena, it is superimposed on the initial image  $I(\tau = -1 \mu s)$  put in transparency (grey levels). Note that  $\tau = 0 \mu s$  is the beginning of the current injection. Two dynamics can be seen. Starting around 13  $\mu s$ , a particle is pulled off from the CFRP and thrown into the cavity (see the circle – particle ejection can be seen in other location but are not shown here). The particle crosses the cavity in about 100  $\mu s$ , at a speed of about 6.5 m/s. On the CFRP side, the persistent red spot indicates a gain in intensity, meaning that matter has been extracting leaving a hole of about 95  $\mu m \times 65 \mu m$  (along x and y respectively). Considering that this particle ejection happens when the current is at its maximum, it can be related to arcing phenomenon in the cavity. Then, on a slower dynamic, the dowel wall (see the arrow) is progressively damaged. To interpret its origin, we define two regions of interest, drawn at  $\tau = 81 \mu s$ ,  $\Omega_1$  at the edge of the dowel and  $\Omega_2$  in the cavity. The averages of  $\Delta I(\tau)$  over  $\Omega_1$  ( $\langle \Delta I(\tau) \rangle_{\Omega_1}$ ) are plotted in Fig. 8. As a reference,  $\langle \Delta I(\tau) \rangle_{\Omega_2}$  (dashed green line) shows the background level inside the cavity. On the other hand, at the dowel interface,

$\langle \Delta I(\tau) \rangle_{\Omega_1}$  (blue solid line) increases until  $\sim 50 \mu\text{s}$  and stabilizes.

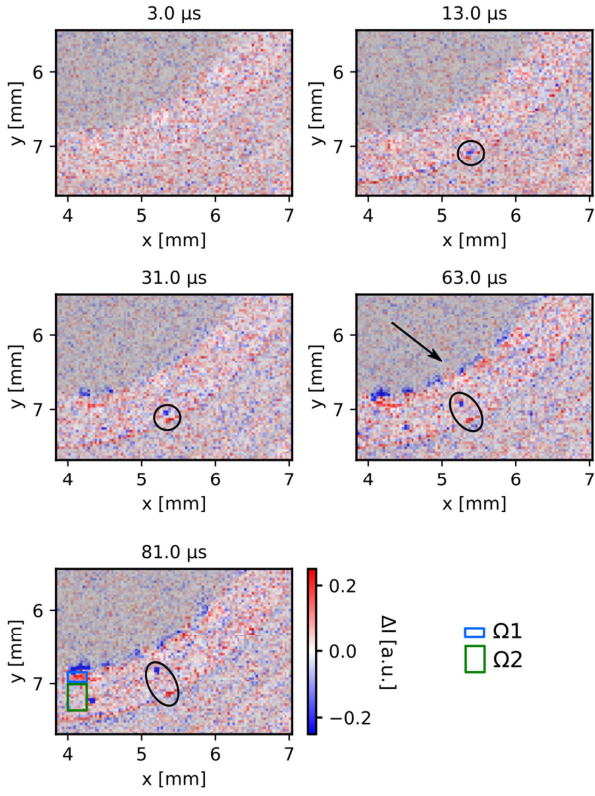


Fig. 7. Dynamic of the fastener cavity during current injection for selected delays in a zoomed area from Fig. 6 (see red dashed box). The injection starts at  $\tau = 0 \mu\text{s}$ . The colour bar corresponds to the difference  $\Delta I(\tau) = I(\tau) - I(\tau = -1 \mu\text{s})$ , where  $I(\tau)$  is the contrast amplitude of the image at the delay  $\tau$ . For reference,  $I(\tau = -1 \mu\text{s})$  is superimposed on  $\Delta I(\tau)$  and is put in transparency (grey background). The circle shows particle ejection, starting around  $13 \mu\text{s}$  and related to arcing. The arrow shows growing damages on the dowel wall. To follow this dynamic, the averages of  $\Delta I(\tau)$  over two regions of interest ( $\Omega_1$  and  $\Omega_2$ ) are reported in Fig. 8.

The dowel interface evolution can be compared to the cumulated electrical energy  $E_{cum}$  deposited as a function of time in the sample.  $E_{cum}(\tau)$  can be calculated as follows :

$$E_{cum}(\tau) = \int V(\tau) \times I(\tau) d\tau \quad (1)$$

where  $V(\tau)$  is the voltage drop between the two fasteners and  $I(t)$  is the pulse of current (Fig. 3).  $V(\tau)$  is measured using the special differential voltage probes described in the reference [2]. Unfortunately, due to the ionizing radiation environment, this measurement could not be performed during the high-speed XPCI measurement, but has been done on a duplicated sample. The time evolution of  $E_{cum}$  is reported in Fig. 8 (dot-dashed black line). One can see that  $E_{cum}$  and  $\langle \Delta I(\tau) \rangle_{\Omega_1}$  have similar trend and  $\langle \Delta I(\tau) \rangle_{\Omega_1}$  stabilises when  $E_{cum}$  is at its maximum (38 J but scaled to  $\langle \Delta I(\tau) \rangle_{\Omega_1}$  to ease the comparison), meaning that the dowel damages are related to the electrical energy deposited in the sample.

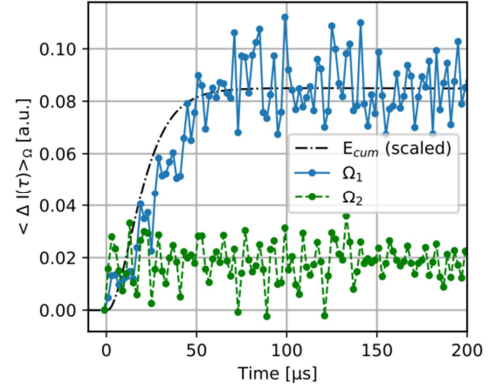


Fig. 8. Average of  $\Delta I(\tau)$  over two regions of interest:  $\Omega_1$  is defined on the fastener wall and  $\Omega_2$  is defined in the cavity for background reference (see Fig. 7). The dynamic trend observed in  $\Omega_1$  is compared to the cumulated electrical energy ( $E_{cum}$ ) deposited in the system.  $E_{cum}$  reaches a maximum of 38 J but is scaled to  $\langle \Delta I(\tau) \rangle_{\Omega_1}$  for comparison.

Among the total electrical energy deposited in the assembly, only a fraction is used to vaporise the Ti dowel. We can estimate this fraction and the vaporised thickness by evaluating the energy contributions at the electrodes using a macroscopic electro-thermal model. Here the anode is the dowel and the cathode is the CFRP. The model is sketched in Fig. 9.

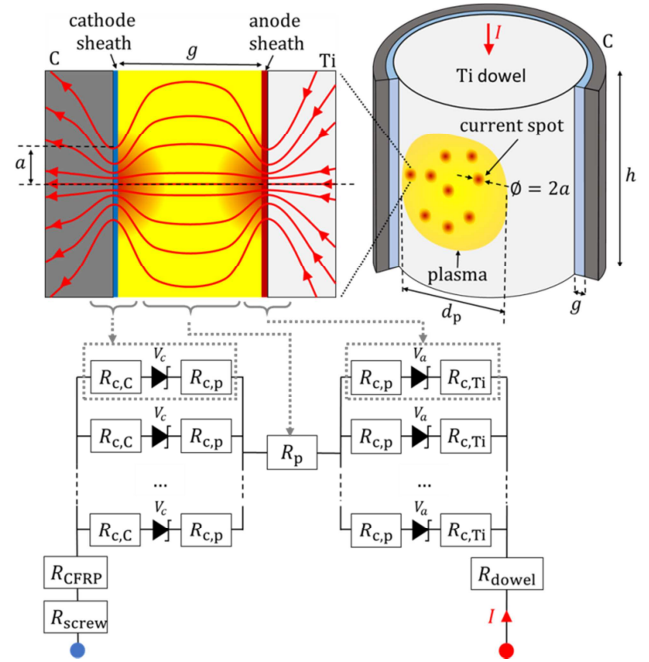


Fig. 9. Sketch of the electro-thermal model showing the macroscopic description of the sparking phenomena.

During the strike, the current flows from the Ti dowel to the CFRP through a plasma filling the cavity gap ( $g$ ). At the interfaces, the current is constricted in a definite number  $N$  of spots which correspond to arc roots. According to the Holm theory [7], we can define for each spot a constriction resistance  $R_{c,j}$  expressed as:

$$R_{c,j} = 1/(4\sigma_j a) \quad (2)$$

where  $\sigma_j$  is the electrical conductivity of titanium (Ti) or plasma (p) or carbon (C) and  $a$  is the spots radius. The  $N$  spots being in parallel, the corresponding equivalent

resistance is  $R_{c,j}/N$ . On the Ti side, this resistance is responsible for local Joule heating. Another source of heat comes from electrons accelerated in the anode sheath which impact the Ti surface and transfer their energy. This energy  $E_{e,a}$  depends on the plasma electronic temperature  $T_e$ , the anode fall  $V_a$  (typically  $\sim 3V$  in our conditions [8] ) and the work function of Ti  $W_{Ti}$ .  $E_{e,a}$  is given by [9] :

$$E_{e,a} = \frac{5}{2} k_B T_e / q_e + V_a + W_{Ti} \quad (3)$$

where  $k_B$  is the Boltzmann constant and  $q_e$  is the elementary electric charge. Considering  $T_e \sim 20000$  K,  $E_{e,a}$  amounts to 11.6 eV.

Thus, the power needed to vaporise Ti over a thickness  $t_v$  at the spots location can be written:

$$\frac{R_{c,Ti}}{N} I(\tau)^2 + I(\tau) E_{e,a} = N \pi a^2 \frac{dt_v(\tau)}{d\tau} (c_{p,Ti} (T_{v,Ti} - T_0) + \Delta H_{f,Ti}^0 + \Delta H_{v,Ti}^0) \rho_{Ti} \quad (4)$$

where  $I(\tau)$  is the pulse of current,  $c_{p,Ti}$  is the specific heat capacity,  $T_{v,Ti}$  and  $T_0$  are the boiling and ambient temperature (respectively),  $\Delta H_{f,Ti}^0$  and  $\Delta H_{v,Ti}^0$  are the latent heats of fusion and vaporisation (respectively) and  $\rho_{Ti}$  is the mass density.

Table 1. Parameters used for the calculations.

$\sigma_{Ti}$	$2.4 \times 10^6 \text{ S.m}^{-1}$	$\sigma_p$	$1 \times 10^4 \text{ S.m}^{-1}$
$T_e$	20000 K	$\sigma_c$	$1 \times 10^4 \text{ S.m}^{-1}$
$V_a$	3 V	$g$	750 $\mu\text{m}$
$W_{Ti}$	4.3 eV	$d_p$	2 mm
$c_{p,Ti}$	$520 \text{ J.kg}^{-1}.\text{K}^{-1}$	$d_{electrodes}$	25 mm
$T_{v,Ti}$	3560 K	$w$	20 mm
$\Delta H_{f,Ti}^0$	$2.95 \times 10^5 \text{ J.kg}^{-1}$	$h$	4.1 mm
$\Delta H_{v,Ti}^0$	$8.9 \times 10^6 \text{ J.kg}^{-1}$	$E_i$	11.3 eV
$\rho_{Ti}$	$4510 \text{ kg.m}^{-3}$	$V_c$	10 V
$\int I(t)^2 dt$	$287 \text{ J.}\Omega^{-1}$	$W_C$	5 eV

One can see in (4) that the vaporised thickness depends strongly on  $a$  – the spot radius – and  $N$  – their number.  $a$  can be reasonably estimated by X-ray imaging to 100  $\mu\text{m}$ . On the other hand, we should set limits to  $N$ . For that, we can compare  $E_{cum}$  with  $E_{tot}$  the energy deposited in the system such that:

$$E_{tot} = R_{tot} \int I(\tau)^2 d\tau + (E_{i,c} + E_{e,a}) \int I(\tau) d\tau, \quad (5)$$

where  $R_{tot}$  is the total resistance of the sample,  $\int I(\tau)^2 d\tau$  is the action integral and  $E_{i,c}$  is energy transferred by ions accelerated in the cathode sheath.  $R_{tot}$  is written as:

$$R_{tot} = (2R_{c,p} + R_{c,c} + R_{c,Ti})/N + R_p + R_{CFRP}. \quad (6)$$

It includes the constriction resistances; the volumetric resistance of the plasma  $R_p = \frac{g}{\pi \sigma_p d_p^2/4}$ , with  $d_p$  the plasma diameter; and the volumetric resistance of the CFRP  $R_{CFRP} = \frac{d_{electrodes}}{\sigma_c w h}$  where  $d_{electrodes}$  is the distance between the electrodes and  $w$  and  $h$  is the width and the height of the CFRP.  $E_{i,c}$  is expressed as [9] :

$$E_{i,c} = (1 - s)(E_i + V_c - W_C) \quad (7)$$

with  $s$  the portion of electronic current at the cathode. According to the Schottky formalism,  $s$  is less than 1% in our conditions.  $E_i$  is the first ionization energy of carbon,  $V_c$  is the cathode fall (typically 10V [8] ) and  $W_C$  is the work

function of carbon. All the parameters for the calculations are listed in Table 1.

We estimate that the energy deposited by charged particles (second term of (5)) amounts to  $\sim 3.5$  J. With  $N$  equals to 10, we get  $R_{tot} \sim 0.13 \Omega$ , leading to  $E_{tot} \sim 41$  J, which is the same order of magnitude as  $E_{cum}$ . As a result, using  $a = 100 \mu\text{m}$  and  $N = 10$  in (4), the first term (joule heating) amounts to 36 mJ whereas the second term amounts to 1.45 J. Indeed, Ti being highly conductive, the joule heating is negligible compare to the sheath effects. The estimated vaporized thickness reaches a plateau of  $\sim 100 \mu\text{m}$  after 80  $\mu\text{s}$ .

This estimation is in agreement with the experimental observations of Fig. 7. The progressive appearance of a fringe on  $\Delta I(\tau)$  indicates that the refractive index gradient at the dowel wall has changed from a solid Ti-air interface to a molten and vaporised Ti-plasma interface. Vaporised Ti extends in the cavity, thus X-ray intensity decreases along the dowel wall (blue signal) and the vapour-plasma interface is emphasized by a localized increased X-ray flux due to ray deviation by phase contrast (red signal). After 80  $\mu\text{s}$ , the vapour width is about 4 pixels corresponding to  $\sim 130 \mu\text{m}$ .

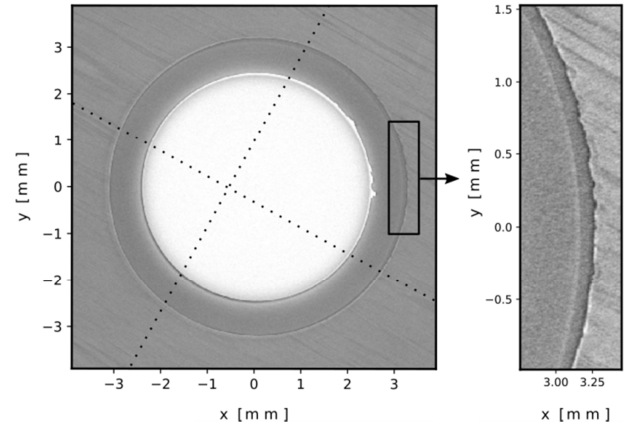


Fig. 10. 6.5  $\mu\text{m}$ -thick XY orthoslice from tomography reconstruction of a similar fastener shot under the same conditions. The noninvasively inspection of the internal damages shows lumps caused by boiling of the fastener wall and carbon extraction on the edge of the CFRP (zoomed area).

Finally, phase contrast tomography is used to noninvasively inspect the internal damages of a similar fastener shot under the same conditions. A 6.5  $\mu\text{m}$ -thick XY orthoslice is extracted from the reconstructed volume and shows a top view of the fastener (see Fig. 10). The contrast is reversed, meaning that the lighter is the grey level, the denser is the area. It can be noted that for this sample the fastener is perfectly centred in the cavity. The slice is taken in a ply oriented at  $-45^\circ$ . As a guide for the reader, the fibres orientation ( $-45^\circ/+45^\circ$ ) is represented by the dotted lines. One can see that the surface of the fastener is damaged only in between the two orientations (right-hand side of the fastener in Fig. 10). Indeed, the current has most likely flown through this area considering the fact that the fibre orientations do not favour any plies and the fastener is centered inside the cavity. The nature of the internal damages confirms the assumptions put forward by the high-speed observations. On the fastener wall, lumps of about 100  $\mu\text{m}$  in thickness can be seen, feature of boiling and re-solidification of a molten layer. On the CFRP side (see the zoomed area),

small cavities ( $\sim 100 \mu\text{m} \times 20 \mu\text{m}$ ) confirm the extraction of matter. In addition, a darker contrast surrounds the cavities. These areas are thus lighter than the non-damaged CFRP. This can come from an increased porosity (formation of carbon powder) or the elimination of the epoxy resin.

## 7. CONCLUSIONS

In the work, the dynamic behaviour of an aeronautical fastener is recorded using non-invasively high-speed XPCI while a 3 kA current pulse is injected. We performed the experiment at the ESRF synchrotron on a dedicated beamline. We identified two kind of damaging processes. The first one, at microsecond timescale, happens when the maximum of current is reached. It is related to arcing phenomenon and results in material extraction of the CFRP cavity wall. The second one, at tens of microsecond timescale, follows the dynamic of electrical energy deposited in the system. It results in melting and boiling of the fastener wall over a depth of about  $120 \mu\text{m}$ . The damages are concentrated where the current has flown, leaving intact most of the fastener and the CFRP cavity surface. The damages are investigated in great details by taking 3D tomograms, to back up the high speed observations. The cavities formed in the CFRP wall are a few tens of micrometre in size. The boiling of the fastener wall gives rise to protrusion of about  $100 \mu\text{m}$ . These create weak points in the assembly where current will be concentrated at the next lightning shock. The experimental observations are compared to an electro-thermal model of electric contact in fastener assembly and used to set limits on some input parameters. To improve the model, a quantitative analysis of the tomographic data will be needed in order to determine the density of a-spots (number of spots per mm) and the volume of damaged material (both for the fastener and the CFRP). This study is the first of its kind. It will need additional experimental sessions to evaluate the influence of different parameters (electrical continuity, cavity gap, plies arrangement...) on the outgassing phenomena.

## 8. REFERENCES

- [1] A. Liebscher et al., "In-situ dynamic pressure and voltage measurement within fastener assemblies during direct lightning attachment tests", *ICOLSE 2017*
- [2] R. Sousa Martins et al., "Characterization of dynamic carbon-metallic contact resistance submitted to a lightning current waveform", *ICOLSE 2019*
- [3] A. Momose, "Recent Advances in X-ray Phase Imaging", *Jpn. J. Appl. Phys.* 44, 6355, 2005
- [4] S. P. Theocharous et al., "Use of synchrotron-based radiography to diagnose pulsed power driven wire explosion experiments", *Rev. Sci. Instrum.* 90, 013504 (2019)
- [5] D. Paganin et al., "Simultaneous phase and amplitude extraction from a single defocused image of a homogeneous object", *Journal of Microscopy* 206, 33-40, 2002
- [6] T. Weitkamp et al., "ANKAphase: software for single-distance phase retrieval from inline X-ray phase-contrast radiographs", *J. Synchrotron Rad.* 18, 617-629, 2011
- [7] R. Holm, "Electric contacts: theory and applications". Springer Verlag GmbH, fourth edition, 1967
- [8] D. J. Dickson and A. von Engel. "Resolving the electrode fall spaces of electric arcs", *Proc. R. Soc. Lond.* A300, 316-325, 1967
- [9] S. Vacquié, "L'arc électrique", p50-56, CNRS editions, 2000

## 9. ACKNOWLEDGEMENTS

We acknowledge the European Synchrotron Radiation Facility for provision of synchrotron radiation facilities and we would like to thank B. Lukic and A. Rack for assistance in using beamline ID19. The authors wish to thank the French Civil Aviation Authority (DGAC) for its support.